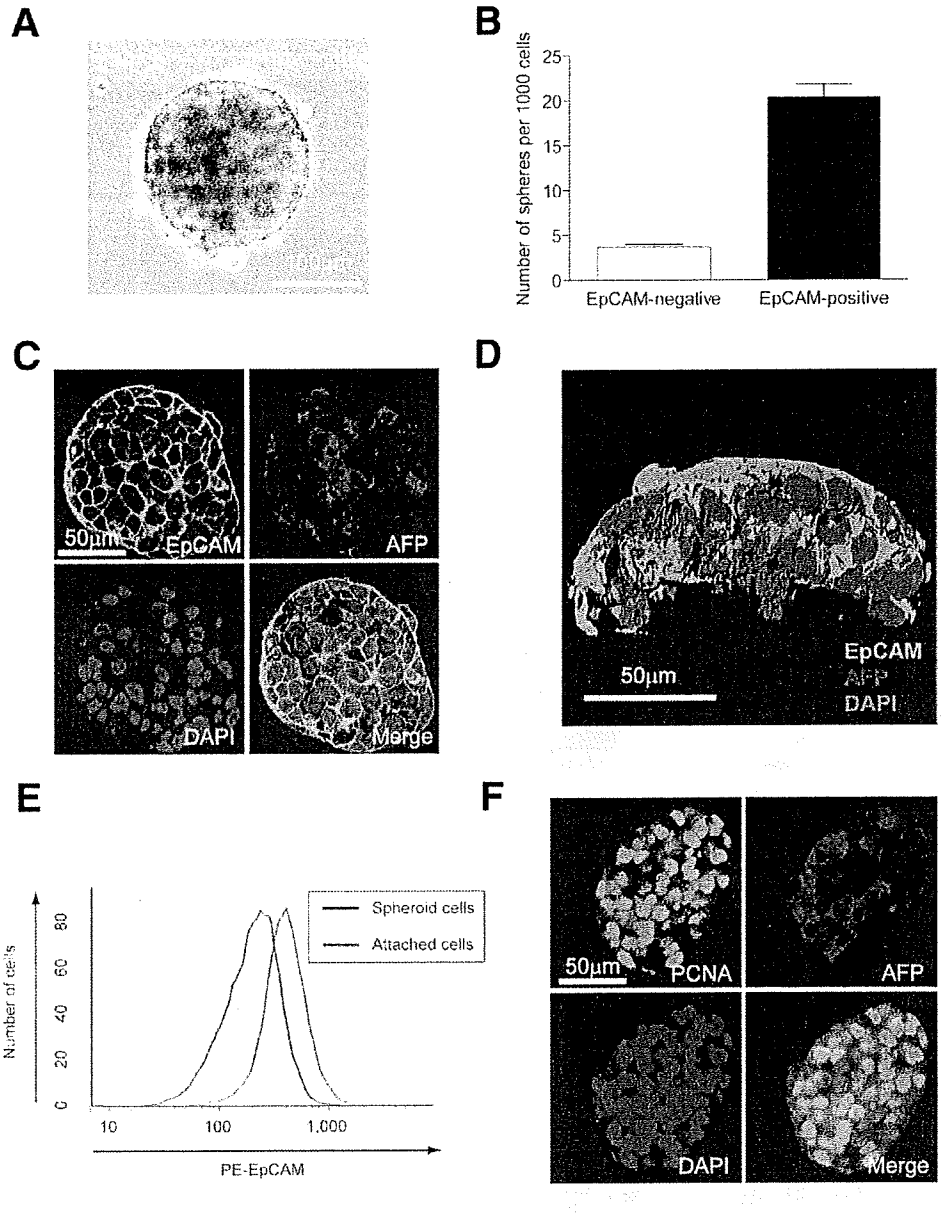

Figure 4. Spheroid formation of EpCAM$^+$ HuH1 HCC cells. (*A*) A representative phase-contrast image of an HCC spheroid derived from an EpCAM$^+$ cell (*scale bar*, 100 μm) and (*B*) total numbers of spheroids from 1000 sorted cells are shown. Experiments were performed in triplicate and data are shown as mean ± SD. (*C*) Representative confocal images of an HCC spheroid co-stained with anti-EpCAM, anti-AFP, and 4′,6-diamidino-2-phenylindole (DAPI) (*scale bar*, 50 μm). (*D*) A 3-dimensional image of an HCC spheroid co-stained with anti-EpCAM, anti-AFP, and DAPI (*scale bar*, 50 μm) reconstructed from confocal images using surface rendering. (*E*) FACS analysis of EpCAM$^+$ cells cultured as spheroid cells (*red*) or attached cells (*blue*) for 14 days after cell sorting. (*F*) Confocal images of an HCC spheroid co-stained with anti-PCNA, anti-AFP, and DAPI (*scale bar*, 50 μm).

However, all colonies were heterogeneous in EpCAM and AFP expression and no colony was completely EpCAM$^-$ (data not shown). Taken together, these results indicate that EpCAM$^+$ HCC cells resemble HpSC features. It appears that EpCAM$^+$ cells, but not EpCAM$^-$ cells, have self-renewal and differentiation capabilities with the ability to form colonies from a single cell, and produce both EpCAM$^+$ and EpCAM$^-$ cells.

It has been shown previously that stem/progenitor cells and cancer stem/progenitor cells can form spheroids in vitro in a nonattached condition.[36,37] Consistently, EpCAM$^+$ cells could form spheroids efficiently, reaching to about 150 to approximately 200 μm in diameter after 14 days of culture (Figure 4*A* and *B*). Interestingly, all cells in a spheroid were EpCAM$^+$, whereas AFP expression was relatively heterogeneous (Figure 4C and *D*, and Supplementary movie 1; see supplementary material online at www.gastrojournal.org). Rarely, a few spheroids derived from an EpCAM$^-$ cell fraction were positive for EpCAM (data not shown), suggesting that these spheroids were derived from contaminated residual EpCAM$^+$ cells by FACS sorting. All spheroid cells maintained EpCAM expression while half of the attached cells lost EpCAM expression when the EpCAM$^+$ fraction was cultured for 14 days (Figure 4*E*). Most spheroid cells also abundantly expressed proliferating cell nuclear antigen (PCNA), implying active cell proliferation (Figure 4*F* and Supplementary movie 2; see supplementary material online at www.gastrojournal.org). Thus, a subset of EpCAM$^+$ cells, but not EpCAM$^-$ cells, can form spheroids.

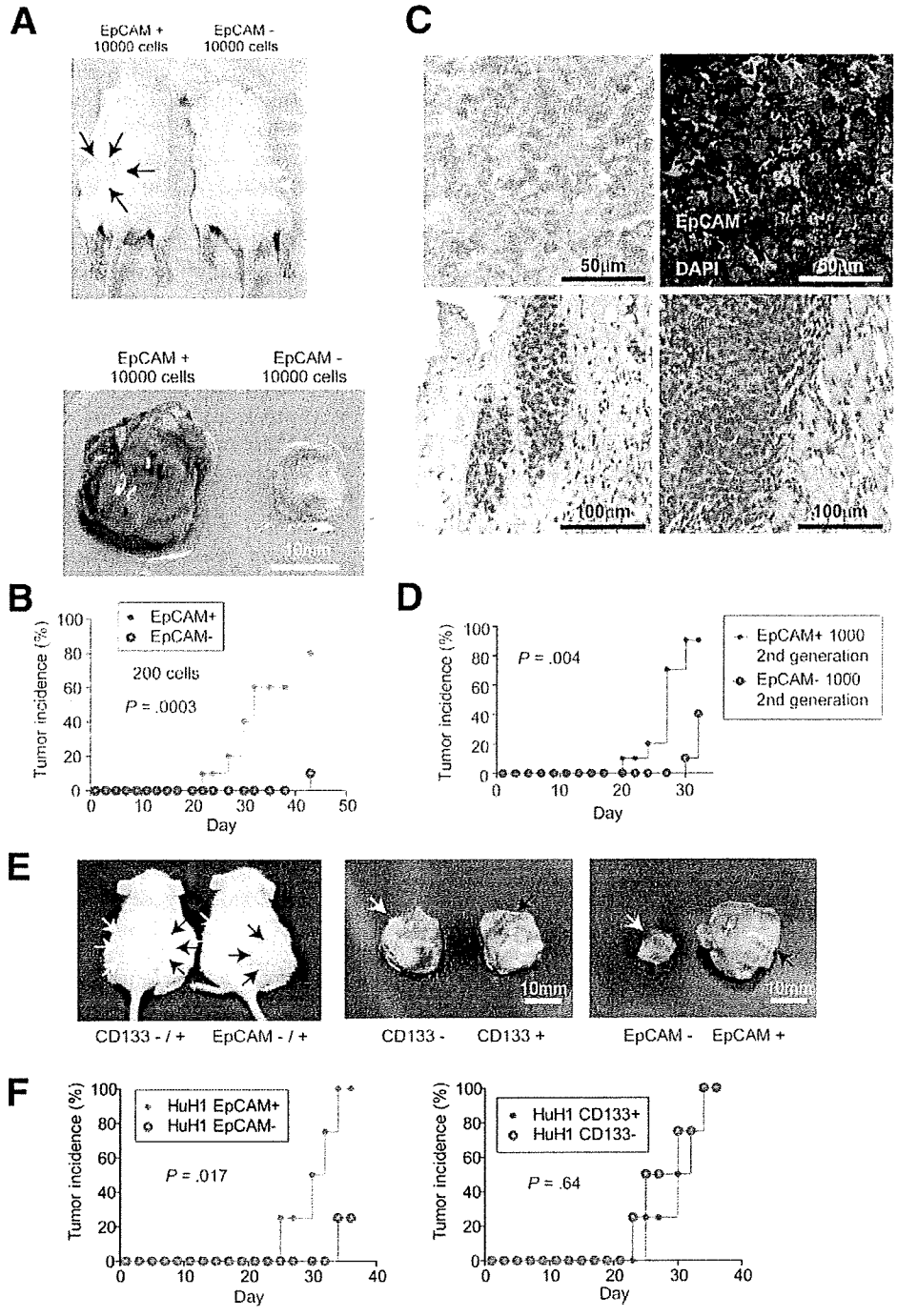

Figure 5. Tumorigenic and invasive potential of EpCAM$^+$ HCC cells. (*A*) Representative NOD/SCID mice (*upper panel*) with subcutaneous tumors (*lower panel*) from EpCAM$^+$ (*black arrows*) or EpCAM$^-$ (*white arrows*) HuH1 cells. (*B*) Tumorigenicity of 200 sorted HuH1 cells. (*C*) Histologic analysis of EpCAM$^+$ HuH1-derived xenografts. H&E staining of a subcutaneous tumor (*left upper panel*) with capsular invasion (*left lower panel*) and muscular invasion (*right lower panel*) and IF of the tumor stained with anti-EpCAM, anti-AFP, and 4′,6-diamidino-2-phenylindole (DAPI) (*right upper panel*) (*scale bar*, 50 μm). (*D*) Tumorigenicity of 1000 sorted cells derived from an EpCAM$^+$ HuH1 xenograft. Data are generated from 10 mice in each group. (*E*) Representative NOD/SCID mice (*left panel*) with subcutaneous tumors from CD133$^+$ (*black arrows*) or CD133$^-$ (*white arrows*) (*middle panel*) and EpCAM$^+$ (black arrows) or EpCAM$^-$ (*white arrows*) (*right panel*) HuH1 cells. (*F*) Tumorigenicity of 1000 HuH1 cells sorted by anti-EpCAM (*left panel*) or anti-CD133 (*right panel*) antibodies.

EpCAM$^+$ HCC Cells as Tumor-Initiating Cells

EpCAM$^+$ HCC cells, but not EpCAM$^-$ HCC cells, could efficiently initiate invasive tumors in NOD/SCID mice (Figure 5). For example, 10,000 EpCAM$^+$ HuH1 cells produced large hypervascular tumors in 100% of mice whereas EpCAM$^-$ cell fractions produced only small and pale-looking tumors in 30% of mice 4 weeks after injection (Figure 5*A* and Supplementary Figure 3*A*; see supplementary material online at www.gastrojournal.org). Similar results were obtained with HuH7 cells (Supplementary Figure 3*B–D*; see supplementary material online at www.gastrojournal.org). As little as 200 EpCAM$^+$ cells could initiate tumors in 8 of 10 injected mice, whereas 200 EpCAM$^-$ cells produced only 1 tumor among 10 injected mice at 6 weeks after transplantation, and the tumor sizes were much larger in the EpCAM$^+$ cells than in the EpCAM$^-$

cells (Figure 5*B* and Supplementary Figure 3*E*; see supplementary material online at www.gastrojournal.org). EpCAM$^+$ cells produced tumors with a mixture of both EpCAM$^+$ and EpCAM$^-$ cells in xenografts, and these cells invaded in the capsule and muscles of the leg adjacent to the tumor (Figure 5*C*). EpCAM$^+$ cells derived from tumors again maintained their tumor-initiating capacity, tumor morphology, and invasive ability in an in vivo serial transplantation experiment (Figure 5*D*). Occasionally, EpCAM$^-$ cell fractions produced a few small tumors that always contained a mixture of EpCAM$^+$ and EpCAM$^-$ cells (data not shown), indicating that the contaminated EpCAM$^+$ cells from FACS sorting contribute to the tumor-initiating ability.

To further validate whether EpCAM$^+$ HCC cells were tumor-initiating cells, we isolated EpCAM$^+$ HCC cells from 2 cases of AFP$^+$ (>600 ng/mL serum AFP) HCC clinical specimens using MACS. Consistently, 1×10^4 EpCAM$^+$ cells could induce tumors in NOD/SCID mice, but up to 1×10^6 EpCAM$^-$ cells failed to do so (Table 1). In addition, similar to HCC cell lines, fresh EpCAM$^+$ tumor cells from 2 clinical HCC specimens were more efficient in forming spheroids in vitro than EpCAM$^-$ cells (Supplementary Figure 4; see supplementary material online at www.gastrojournal.org).

FACS analysis results indicate that a majority of EpCAM$^+$ cells express CD133 in HuH7 cells but not in HuH1 cells (Figure 2*B*), which prompted us to compare the tumorigenic capacity of EpCAM$^+$ and CD133$^+$ cells in these cell lines. Noticeably, EpCAM$^+$ HuH1 cells showed marked tumor-initiating capacity compared with CD133$^+$ HuH1 cells (Figure 5*E* and *F*), whereas EpCAM$^+$ and CD133$^+$ cells had similar tumorigenic ability in HuH7 cells (data not shown).

GSK-3β Inhibition Augments EpCAM$^+$ HCC Cells

To determine the role of Wnt/β-catenin signaling[28] in EpCAM$^+$ HCC cells (Figure 1*B*), we first treated HuH1, HuH7, and HLF cells with a GSK-3β inhibitor BIO (Figure 6*A*), which activates Wnt/β-catenin signaling (Figure 6*B*) and maintains undifferentiation of embryonic stem cells.[38] 6-bromoindirubin-3′-oxime (BIO) increased the EpCAM$^+$ cell population in HuH1 and HuH7 cells when compared with the control methylated BIO (MeBIO) (Figure 6*A*). In contrast, BIO had no effect on the CD90$^+$ cell population, which is more tumorigenic than the CD90$^-$ cell population in HLF (Figure 6*A* and data not shown). Enrichment of EpCAM$^+$ cells was provoked further by the treatment of Wnt10B-conditioned media in HuH7 cells (Figure 6*C*).[34] BIO induced morphologic alteration of HuH7 cells because most cells became small and round when compared with MeBIO and suppressed EpCAM$^-$ AFP$^-$ cell populations (Figure 6*D*). Moreover, BIO induced *TACSTD1*, *MYC*, and *hTERT* expression and spheroid formation (Figure 6*E* and *F*).

Table 1. The Tumor-Initiating Capacity of EpCAM$^+$ Cells From Clinical HCC Specimens

HCC patients				Tumor incidence (mice with tumors/total no. of mice injected)	
No.	% of EpCAM$^+$ HCC cells	Groups	No. of cells injected	2 months	3 months
1	5.2	EpCAM$^+$	1×10^3	0/3	0/3
			1×10^4	2/3	2/3
			1×10^5	2/2	2/2
		EpCAM$^-$	1×10^5	0/3	0/3
			1×10^6	0/2	0/2
2	1.4	EpCAM$^+$	1×10^3	0/2	0/2
			1×10^4	0/1	1/1
		EpCAM$^-$	1×10^4	0/3	0/3
			1×10^5	0/2	0/2

EpCAM Blockage by RNA Interference

One of the hallmarks of CSCs is its resistance to conventional chemotherapeutic agents resulting in tumor relapse and thus targeting CSCs is critical to achieve successful tumor remission. Consistently, 5-FU could increase the EpCAM$^+$ population and spheroid formation of HuH1 and HuH7 cells (Figure 7*A* and *B*) (data not shown), suggesting a differential sensitivity of EpCAM$^+$ and EpCAM$^-$ HCC cells to 5-FU. In contrast, EpCAM blockage via RNA interference dramatically decreased the population of EpCAM$^+$ cells (Figure 7*C*), and significantly inhibited cellular invasion, spheroid formation, and tumorigenicity of HuH1 cells (Figure 7*D–F*). Thus, EpCAM may serve as a molecular target to eliminate HCC cells with stem/progenitor cell features.

Discussion

The cellular origin of HCC is currently in debate. In this study, we found that EpCAM can serve as a marker to enrich HCC cells with tumor-initiating ability and with some stem/progenitor cell traits. EpCAM is expressed in many human cancers with an epithelial origin.[39] During embryogenesis, EpCAM is expressed in fertilized oocytes, embryonic stem cells, and embryoid bodies, suggesting its role in early stage embryogenesis.[40] Furthermore, a recent article indicated that EpCAM is expressed in colonic and breast CSCs.[41] Taken together, these data suggest a critical role of EpCAM in CSCs as well as embryonic and somatic stem cells. Consistently, we found that EpCAM expression is regulated by Wnt/β-catenin signaling[29] and tumorigenic and highly invasive HpSC-HCC is orchestrated by a subset of cells expressing EpCAM and AFP with stem cell–like features and self-renewal and differentiation capabilities regulated by Wnt/β-catenin signaling (this study). Thus, EpCAM may be a common gene expressed in undifferentiated normal cells and HCCs with activated Wnt/β-catenin signaling. It may act as a downstream molecule

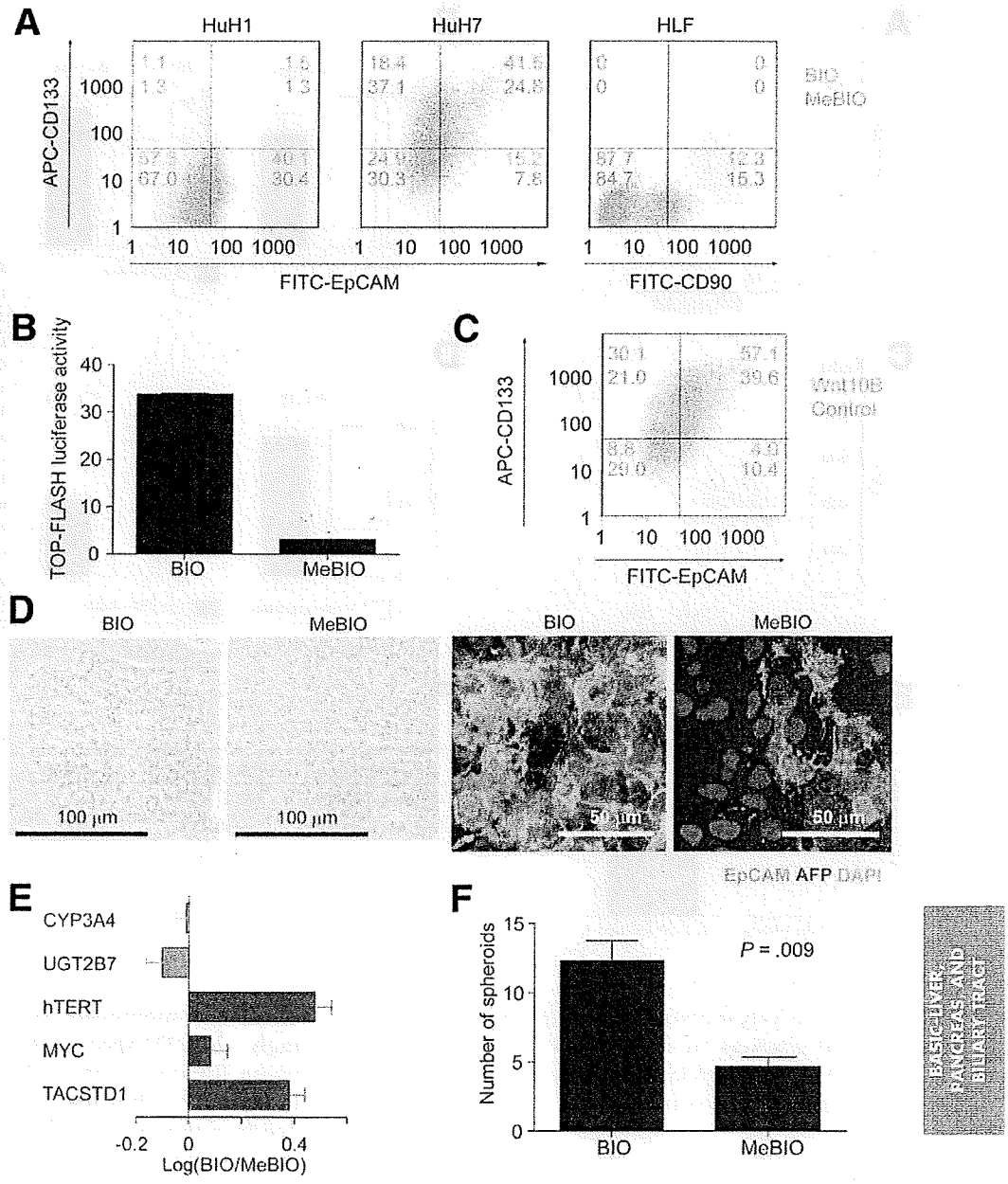

Figure 6. Wnt/β-catenin signaling augments EpCAM+ HCC cells. (*A*) Flow cytometer analysis of HuH1, HuH7, and HLF cells treated with 2 μmol/L of BIO (*orange*) or MeBIO (*green*) for 10 days and stained with anti-EpCAM, anti-CD133 and anti-CD90 antibodies. (*B*) TOP-FLASH luciferase assays of HuH7 cells treated with 2 μmol/L of BIO or MeBIO. (*C*) Flow cytometer analysis of HuH7 cells cultured in normal media (Dulbecco's modified Eagle medium supplemented with 10% FBS) or Wnt10B conditioned media (details are described in the Materials and Methods section). Cells were cultured in each medium for 2 weeks. (*D*) Representative phase-contrast images (*left panel*: *scale bar*, 100 μm) or IF images (*right panel*: *scale bar*, 50 μm) of HuH7 cells treated with 2 μmol/L of BIO or MeBIO for 14 days. (*E*) Quantitative reverse transcription-polymerase chain reaction analysis of representative HpSC-HCC–related genes in HuH7 cells treated with 2 μmol/L of BIO or MeBIO for 14 days. (*F*) Spheroid formation assay of HuH7 cells treated with 2 μmol/L of BIO or MeBIO for 14 days (mean ± SD). FITC, fluorescein isothiocyanate.

to maintain HCC stemness and serve as a good marker for HCC initiating cells.

CD133 or CD90 have been used to identify potential hepatic CSCs.[35,42] CD133 is expressed in normal and malignant stem cells of the neural, hematopoietic, epithelial, hepatic, and endothelial lineages,[23,43,44] suggesting that CD133 is also a common marker to detect normal cells and CSCs. Captivatingly, EpCAM expression overlaps with CD133 expression in normal human colon tissues and colorectal cancer tissues, yet CD133+ and CD133− cells are equally tumorigenic.[45] Similarly, we found that EpCAM+ and EpCAM− HuH1 cells equally expressed CD133, but only EpCAM+ cells developed large hypervascular tumors. Our data suggest that EpCAM may be a better marker than CD133 to enrich HCC tumor-initiating cells from AFP+ tumors. We also found that CD90 expression was limited to HCC cell lines that are EpCAM− AFP−, and Wnt/β-catenin signaling had little effect on CD90+ cell enrichment. These results suggest that the expression patterns of various stem cell markers in tumor-initiating cells with stem/progenitor cell features may be different in each HCC subtype, possibly owing to the heterogeneity of activated signaling pathways in normal stem/progenitor cells where these tumor-initiating cells may originate. Therefore, it would be useful to

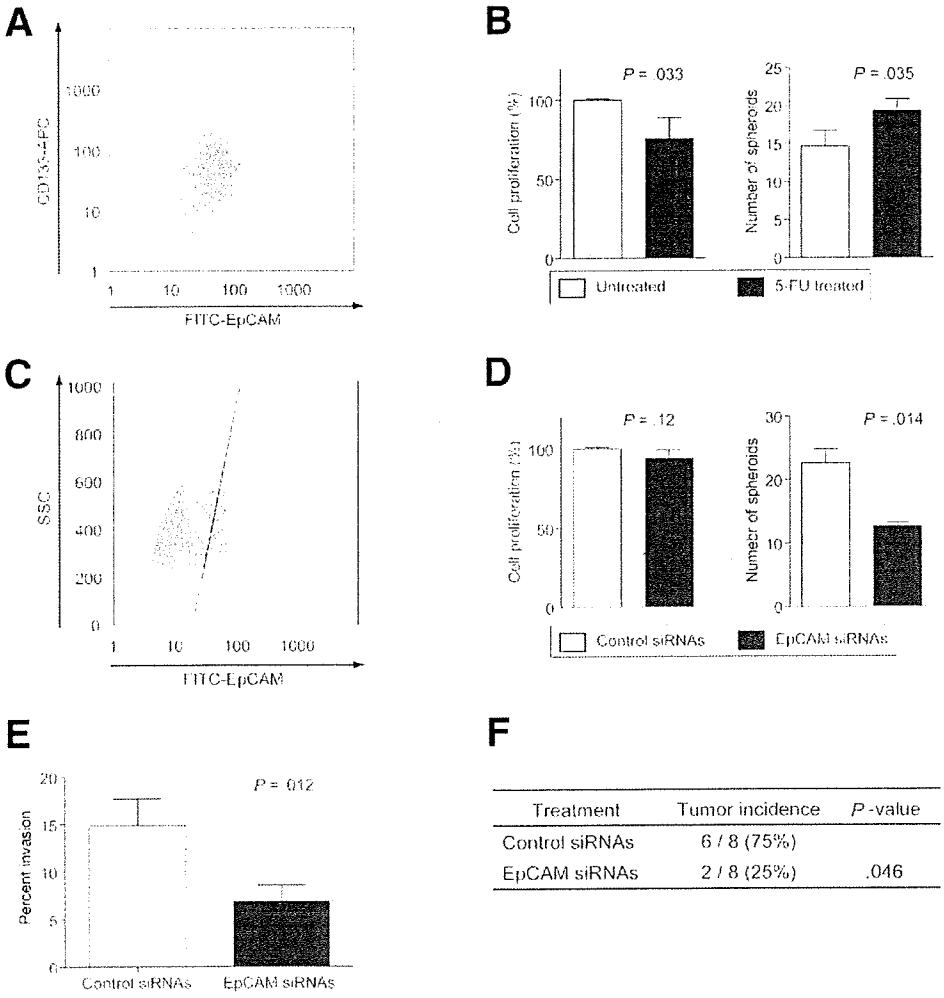

F

Treatment	Tumor incidence	*P*-value
Control siRNAs	6 / 8 (75%)	
EpCAM siRNAs	2 / 8 (25%)	.046

Figure 7. EpCAM blockage inhibits the tumorigenic and invasive capacity of EpCAM$^+$ HCC cells. (*A*) Enrichment of EpCAM$^+$ cells after 5-FU treatment. HuH1 cells refer as control or without treatment (*green*) or treated with 2 μg/mL of 5-FU (*orange*) for 3 days and analyzed by FACS using anti-EpCAM and anti-CD133 antibodies. (*B*) Spheroid formation of HuH1 cells treated with 2 μg/mL of 5-FU for 3 days. (*C*) FACS analysis of HuH1 cells treated with a control siRNA (orange) or EpCAM-specific siRNA (*green*) at day 3 after transfection. (*D*) Spheroid formation or (*E*) invasive capacity ofEpCAM$^+$ HuH1 cells transfected with a control siRNA or EpCAM-specific siRNA. Experiments were performed in triplicate and the data are shown as mean ± SD. (*D*) siRNAs. (*F*) Inhibition of tumor formation in vivo by EpCAM gene silencing. EpCAM$^+$ HuH1 cells were transfected with siRNA oligos and 1000 cells were injected 24 hours after transfection.

comprehensively investigate the expression patterns of stem cell markers to characterize the population of CSCs that may correlate with the activation of their distinct molecular pathways.

CSCs may be more resistant to chemotherapeutic agents than differentiated tumor cells possibly owing to an increased expression of adenosine triphosphate-binding cassette transporters and anti-apoptotic proteins.[4] Thus, the development of an effective strategy to target CSC pools together with conventional chemotherapies is essential to eradicate a tumor mass.[14] By blocking the programs that activate self-renewal and/or inhibit asymmetric division, CSC features could be destemmed.[46,47] Consistently, EpCAM blockage could inhibit cellular invasion and tumorigenicity of EpCAM$^+$ HCC cells, revealing the feasibility of targeting a CSC marker to destem CSC features. EpCAM may induce c-Myc,[48] a common molecular node activated in HpSC-HCC.[27] c-Myc, together with Oct3/4, Sox2, and Klf4, can induce pluripotent stem cells from adult fibroblasts.[49] It is possible that EpCAM blockage to inhibit hepatic CSCs may result in a suppression of c-Myc signaling. Encouragingly, EpCAM-specific antibodies are currently in phase II clinical trials.[50] Furthermore, a recent study indicated that EpCAM$^+$ circulating tumor cells identified by a unique microfluidic platform can be used to monitor outcomes of patients undergoing systemic treatment.[51] Therefore, it may be useful to combine EpCAM antibodies with conventional chemotherapy to target both CSCs and non-CSCs for the treatment of HCC.

Supplementary Data

Note: To access the supplementary material accompanying this article, visit the online version of *Gastroenterology* at www.gastrojournal.org, and at doi: 10.1053/j.gastro.2008.12.004.

References

1. Fialkow PJ. Clonal origin of human tumors. Biochim Biophys Acta 1976;458:283–321.

2. Heppner GH. Tumor heterogeneity. Cancer Res 1984;44:2259–2265.
3. Hanahan D, Weinberg RA. The hallmarks of cancer. Cell 2000;100:57–70.
4. Jordan CT, Guzman ML, Noble M. Cancer stem cells. N Engl J Med 2006;355:1253–1261.
5. Clarke MF, Dick JE, Dirks PB, et al. Cancer stem cells—perspectives on current status and future directions: AACR Workshop on cancer stem cells. Cancer Res 2006;66:9339–9344.
6. Potter VR. Phenotypic diversity in experimental hepatomas: the concept of partially blocked ontogeny. The 10th Walter Hubert Lecture. Br J Cancer 1978;38:1–23.
7. Sell S. Cellular origin of cancer: dedifferentiation or stem cell maturation arrest? Environ Health Perspect 1993;101(Suppl 5):15–26.
8. Wicha MS, Liu S, Dontu G. Cancer stem cells: an old idea—a paradigm shift. Cancer Res 2006;66:1883–1890.
9. Al Hajj M, Wicha MS, Benito-Hernandez A, et al. Prospective identification of tumorigenic breast cancer cells. Proc Natl Acad Sci U S A 2003;100:3983–3988.
10. Singh SK, Hawkins C, Clarke ID, et al. Identification of human brain tumour initiating cells. Nature 2004;432:396–401.
11. Bonnet D, Dick JE. Human acute myeloid leukemia is organized as a hierarchy that originates from a primitive hematopoietic cell. Nat Med 1997;3:730–737.
12. Ricci-Vitiani L, Lombardi DG, Pilozzi E, et al. Identification and expansion of human colon-cancer-initiating cells. Nature 2007;445:111–115.
13. O'Brien CA, Pollett A, Gallinger S, et al. A human colon cancer cell capable of initiating tumour growth in immunodeficient mice. Nature 2007;445:106–110.
14. Dean M, Fojo T, Bates S. Tumour stem cells and drug resistance. Nat Rev Cancer 2005;5:275–284.
15. Rich JN. Cancer stem cells in radiation resistance. Cancer Res 2007;67:8980–8984.
16. Parkin DM, Bray F, Ferlay J, et al. Global cancer statistics, 2002. CA Cancer J Clin 2005;55:74–108.
17. Sell S, Pierce GB. Maturation arrest of stem cell differentiation is a common pathway for the cellular origin of teratocarcinomas and epithelial cancers. Lab Invest 1994;70:6–22.
18. Thorgeirsson SS, Grisham JW. Hepatic stem cells. Semin Liver Dis 2003;23:301.
19. Thorgeirsson SS, Grisham JW. Molecular pathogenesis of human hepatocellular carcinoma. Nat Genet 2002;31:339–346.
20. Lee JS, Heo J, Libbrecht L, et al. A novel prognostic subtype of human hepatocellular carcinoma derived from hepatic progenitor cells. Nat Med 2006;12:410–416.
21. Sigal SH, Brill S, Fiorino AS, et al. The liver as a stem cell and lineage system. Am J Physiol 1992;263:G139–G148.
22. Schmelzer E, Wauthier E, Reid LM. The phenotypes of pluripotent human hepatic progenitors. Stem Cells 2006;24:1852–1858.
23. Schmelzer E, Zhang L, Bruce A, et al. Human hepatic stem cells from fetal and postnatal donors. J Exp Med 2007;204:1973–1987.
24. Dan YY, Riehle KJ, Lazaro C, et al. Isolation of multipotent progenitor cells from human fetal liver capable of differentiating into liver and mesenchymal lineages. Proc Natl Acad Sci U S A 2006;103:9912–9917.
25. Zaret KS. Regulatory phases of early liver development: paradigms of organogenesis. Nat Rev Genet 2002;3:499–512.
26. Shafritz DA, Oertel M, Menthena A, et al. Liver stem cells and prospects for liver reconstitution by transplanted cells. Hepatology 2006;43:S89–S98.
27. Yamashita T, Forgues M, Wang W, et al. EpCAM and alpha-fetoprotein expression defines novel prognostic subtypes of hepatocellular carcinoma. Cancer Res 2008;68:1451–1461.
28. Reya T, Clevers H. Wnt signalling in stem cells and cancer. Nature 2005;434:843–850.
29. Yamashita T, Budhu A, Forgues M, et al. Activation of hepatic stem cell marker EpCAM by Wnt-β-catenin signaling in hepatocellular carcinoma. Cancer Res 2007;67:10831–10839.
30. Budhu A, Forgues M, Ye QH, et al. Prediction of venous metastases, recurrence and prognosis in hepatocellular carcinoma based on a unique immune response signature of the liver microenvironment. Cancer Cell 2006;10:99–111.
31. Ye QH, Qin LX, Forgues M, et al. Predicting hepatitis B virus-positive metastatic hepatocellular carcinomas using gene expression profiling and supervised machine learning. Nat Med 2003;9:416–423.
32. Wu CG, Forgues M, Siddique S, et al. SAGE transcript profiles of normal primary human hepatocytes expressing oncogenic hepatitis B virus X protein. FASEB J 2002;16:1665–1667.
33. Kubota H, Reid LM. Clonogenic hepatoblasts, common precursors for hepatocytic and biliary lineages, are lacking classical major histocompatibility complex class I antigen. Proc Natl Acad Sci U S A 2000;97:12132–12137.
34. Yoshikawa H, Matsubara K, Zhou X, et al. WNT10B functional dualism: beta-catenin/Tcf-dependent growth promotion or independent suppression with deregulated expression in cancer. Mol Biol Cell 2007;18:4292–4303.
35. Yang ZF, Ho DW, Ng MN, et al. Significance of CD90(+) cancer stem cells in human liver cancer. Cancer Cell 2008;13:153–166.
36. Dontu G, Abdallah WM, Foley JM, et al. In vitro propagation and transcriptional profiling of human mammary stem/progenitor cells. Genes Dev 2003;17:1253–1270.
37. Fang D, Nguyen TK, Leishear K, et al. A tumorigenic subpopulation with stem cell properties in melanomas. Cancer Res 2005;65:9328–9337.
38. Sato N, Meijer L, Skaltsounis L, et al. Maintenance of pluripotency in human and mouse embryonic stem cells through activation of Wnt signaling by a pharmacological GSK-3-specific inhibitor. Nat Med 2004;10:55–63.
39. Balzar M, Winter MJ, de Boer CJ, et al. The biology of the 17-1A antigen (Ep-CAM). J Mol Med 1999;77:699–712.
40. Trzpis M, McLaughlin PM, de Leij LM, et al. Epithelial cell adhesion molecule: more than a carcinoma marker and adhesion molecule. Am J Pathol 2007;171:386–395.
41. Dalerba P, Dylla SJ, Park IK, et al. Phenotypic characterization of human colorectal cancer stem cells. Proc Natl Acad Sci U S A 2007;104:10158–10163.
42. Ma S, Chan KW, Hu L, et al. Identification and characterization of tumorigenic liver cancer stem/progenitor cells. Gastroenterology 2007;132:2542–2556.
43. Yin AH, Miraglia S, Zanjani ED, et al. AC133, a novel marker for human hematopoietic stem and progenitor cells. Blood 1997;90:5002–5012.
44. Fargeas CA, Corbeil D, Huttner WB. AC133 antigen, CD133, prominin-1, prominin-2, etc.: prominin family gene products in need of a rational nomenclature. Stem Cells 2003;21:506–508.
45. Shmelkov SV, Butler JM, Hooper AT, et al. CD133 expression is not restricted to stem cells, and both CD133+ and CD133- metastatic colon cancer cells initiate tumors. J Clin Invest 2008;118:2111–2120.
46. Hill RP, Perris R. "Destemming" cancer stem cells. J Natl Cancer Inst 2007;99:1435–1440.
47. Piccirillo SG, Reynolds BA, Zanetti N, et al. Bone morphogenetic proteins inhibit the tumorigenic potential of human brain tumour-initiating cells. Nature 2006;444:761–765.
48. Munz M, Kieu C, Mack B, et al. The carcinoma-associated antigen EpCAM upregulates c-myc and induces cell proliferation. Oncogene 2004;23:5748–5758.

49. Takahashi K, Tanabe K, Ohnuki M, et al. Induction of pluripotent stem cells from adult human fibroblasts by defined factors. Cell 2007;131:861–872.
50. Chaudry MA, Sales K, Ruf P, et al. EpCAM an immunotherapeutic target for gastrointestinal malignancy: current experience and future challenges. Br J Cancer 2007;96:1013–1019.
51. Nagrath S, Sequist LV, Maheswaran S, et al. Isolation of rare circulating tumour cells in cancer patients by microchip technology. Nature 2007;450:1235–1241.

Received March 9, 2008. Accepted December 1, 2008.

Reprint requests

Address requests for reprints to: Xin Wei Wang, PhD, Liver Carcinogenesis Section, Laboratory of Human Carcinogenesis, Center for Cancer Research, National Cancer Institute, 37 Convent Drive, Building 37, Room 3044A, MSC 4258, Bethesda, Maryland 20892-4258. e-mail: **xw3u@nih.gov; fax: (301) 496-0497.**

Acknowledgments

Microarray data are available publicly at http://www.ncbi.nlm.nih.gov/geo/ (accession number: GSE5975).

The authors thank Drs Curtis Harris and Sharon Pine for critical readings of the manuscript; Ms Barbara Taylor and Dr Susan Garfield for technical assistance; Drs Ali Brivanlou (Rockefeller University), Steve Strom (University of Pittsburgh), and Bert Vogelstein (Johns Hopkins University) for generously providing their research materials.

Conflicts of interest

The authors disclose no conflicts.

Funding

The authors disclose the following: This work was supported in part by the Intramural Research Program of the Center for Cancer Research, the US National Cancer Institute. Dr Yang, Dr HY Wang, Dr Jia, Dr Ye, Dr Qin, and Dr Tang were supported by research grants from the China National Natural Science Foundation for Distinguished Young Scholars (30325041) and the China National "863" R&D High-Tech Key Project (2002BA711A02-4). Dr Reid was supported by a sponsored research grant from Vesta Therapeutics (Research Triangle Park, NC), National Institutes of Health grants (RO1 AA014243 and RO1 IP30-DK065933), and a US Department of Energy grant (DE-FG02-02ER-63477). Sponsors had no role in the study design, data collection, analysis, and interpretation. Dr Yamashita, Dr Ji, Dr Budhu, Dr Forgues, Dr Yang, Dr Wang, Dr Jia, Dr Ye, Dr Wauthier, Dr Minato, Dr Honda, Dr Kaneko, and Dr Wang disclose no conflicts.

Supplementary Materials and Methods

FACS and MACS Analyses

Cultured cells were trypsinized, washed, and resuspended in Hank's balanced salt solutions (Lonza, Basel, Switzerland) supplemented with 1% HEPES and 2% fetal bovine serum. Cells then were incubated with FITC-conjugated anti-EpCAM monoclonal antibody Clone Ber-EP4 (DAKO, Carpinteria, CA) on ice for 30 minutes, and $EpCAM^+$ and EpCAM cells were isolated by a BD FACSAria cell sorting system (BD Biosciences). For magnetic separation, cells were labeled 24 hours after enzymatic dissociation with primary EpCAM antibody (mouse IgG1; Dako), subsequently magnetically labeled with rat anti-mouse IgG1 Microbeads, and separated on a MACS LS column (Miltenyi Biotec, Inc, Auburn, CA). All the procedures were performed according to the manufacturer's instructions. The purity of sorted cells was evaluated by FACS. Fixed cells also were analyzed by FACS using a FACSCalibur (BD Biosciences). Anti-EpCAM antibody VU-1D9, anti-CD133/2 clone 293C3 (Miltenyi Biotec Inc), and anti-CD90 clone 5E10 (StemCell Technologies Inc, Vancouver, British Columbia, Canada) were used to detect $EpCAM^+$, $CD133^+$, or $CD90^+$ cells. Intracellular AFP levels were examined by a BD Cytofix/Cytoperm Fixation/Permeabilization Kit (San Jose, CA) and anti-AFP rabbit polyclonal antibody (DAKO).

Quantitative Reverse Transcription–Polymerase Chain Reaction and IHC Analyses

Total RNA was extracted using TRIzol (Invitrogen) according to the manufacturer's instructions. The expression of selected genes was determined in triplicate using the Applied Biosystems 7500 Sequence Detection System (Applied Biosystems, Foster City, CA) as previously described.[1] Genes expressed in embryonic stem cells were determined in quadruplicate using TaqMan Human Stem Cell Pluripotency Array (Applied Biosystems). IHC analyses with specific antibodies were performed essentially as previously described.[1] Confocal fluorescence microscopic analysis was performed essentially as previously described.[2]

References

1. Yamashita T, Forgues M, Wang W, et al. EpCAM and alpha-fetoprotein expression defines novel prognostic subtypes of hepatocellular carcinoma. Cancer Res 2008;68:1451–1461.
2. Wang W, Budhu A, Forgues M, et al. Temporal and spatial control of nucleophosmin by the Ran-Crm1 complex in centrosome duplication. Nat Cell Biol 2005;7:823–830.

Supplemetary Table 1. Clinicopathologic Characteristics of HpSC-HCC and MH-HCC Cases Used for Oligonucleotide Microarray Analyses

Parameters	HpSC-HCC (n = 60)	MH-HCC (n = 96)	*P* value[a]
Mean age, *y* (SD)	46.0 ± 10.7	52.9 ± 10.5	.0004
Sex: male/female	50/10	87/9	.18
Cirrhosis: yes/no/no data	56/4	88/7/1	.72
Median AFP level, *ng/mL* (25%–75%)	1706 (865–5915)	11.8 (4.0–48.6)	<.0001
Histologic grade[b]			
I–II	14	41	
II–III	44	48	
III–IV	2	5	
No data	0	2	.031
Mean tumor size, *cm* (SD)	5.1 ± 3.0	4.4 ± 3.0	.088
Multinodular: yes/no	16/44	15/81	.09
Portal vein invasion, yes/no[c]	11/49	9/87	.10
TNM classification			
I	24	46	
II	22	42	
III	14	8	.03
Virus status: HBV/HBV + HCV/unknown	56/4/0	95/0/1	.43

[a]Mann–Whitney *U* test or χ^2 test.
[b]Edmondson–Steiner.
[c]Macroscopic portal vein invasion.

Supplementary Table 2. Clinicopathologic Characteristics of HpSC-HCC and MH-HCC Cases Used for IHC

Parameters	HpSC-HCC (n = 24)	MH-HCC (n = 55)	*P* value[a]
Mean age, *y* (SD)	46.4 ± 9.4	58.4 ± 11.9	<.0001
Sex: male/female	20/4	48/7	.64
Cirrhosis: yes/no	23/1	46/9	.14
Median AFP level, *ng/mL* (25%–75%)	1620 (887–3166)	12 (9.3–219)	<.0001
Histologic grade[b]			
I–II	12	32	
II–III	8	21	
III–IV	4	2	.13
Mean tumor size, *cm* (SD)	7.1 ± 3.6	5.2 ± 3.6	.014
Multinodular: yes/no	4/20	16/39	.24
Portal vein invasion: yes/no[c]	12/12	12/43	.012
TNM classification			
I	4	19	
II	8	20	
III	12	16	.14
Virus status: HBV/HCV/unknown	21/2/1	32/21/2	.026

[a]Mann–Whitney *U* test or χ^2 test.
[b]Edmondson–Steiner.
[c]Macroscopic portal vein invasion.

Supplementary Table 3. Top 10 List of Canonical Pathways Activated in HpSC-HCC From Ingenuity Pathway Analysis

Pathways	Genes included in cluster A
Axonal guidance signaling	
Up	ROBO2, ARPC5L (includes EG:81873), SEMA4G, PDGFRB, PLCB1, PRKCD, FGFR3, FZD5, MERTK, DDR1, LINGO1, SEMA3C
Down	PIK3C3, IGF1, PIK3C2G, MAP2K2, ARHGEF15
Transforming growth factor-β signaling	
Up	PDGFRB, FGFR3, MERTK, UBD, DDR1, SMAD5
Down	MAP2K2, HNF4A
Integrin signaling	
Up	ARPC5L (includes EG:81873), PDGFRB, FGFR3, GRB7, MERTK, ITGB5, DDR1, DDEF1
Down	PIK3C3, MYLK, PIK3C2G, MAP2K2
Apoptosis signaling	
Up	PDGFRB, BAK1, CYCS, FGFR3, MERTK, DDR1
Down	MAP3K5, MAP2K2
G2/M DNA damage checkpoint regulation	
Up	YWHAZ, CCNB2, UBD, WEE1
Down	CDKN2A, GADD45A
ERK/MAPK signaling	
Up	ELF3, PDGFRB, YWHAZ, PRKCD, FGFR3, MERTK, DDR1
Down	PIK3C3, DUSP1, PIK3C2G, ESR1, MAP2K2
Wnt/β-catenin signaling	
Up	DKK1, SOX9, FZD5, UBD, TCF7L2, CSNK1E
Down	CDKN2A, RARG
PI3K/AKT signaling	
Up	PDGFRB, YWHAZ, FGFR3, MERTK, DDR1
Down	MAP3K5, MAP2K2, GYS2
Amyloid processing	
Up	BACE2, CSNK1E, MAPK13
Down	
Leukocyte extravasation signaling	
Up	PRKCD, CLDN4, CLDN1, MMP11, MAPK13
Down	PIK3C3, CLDN2, PIK3C2G, MAP2K2

NOTE. The top 10 pathways were selected based on the significance for the enrichment of the genes with a particular canonical signaling pathway determined by the one-sided Fisher exact test ($P < .01$).

Supplementary Table 4. Top 10 List of Canonical Pathways Activated in MH-HCC From Ingenuity Pathway Analysis

Pathways	Genes included in cluster B
Lipopolysaccharide/interleukin-1–mediated inhibition of RXR function	
Up	SULT1C2, ACSL4, ACSL3, FABP5, GSTP1
Down	NR1I2, NR1I3, CYP7A1, ALDH1L1, ABCB1, SLC10A1, SLC27A2, CD14, GSTM1, ALDH6A1, GSTM4, ACSL5, CES2 (includes EG:8824), FMO3, SULT2A1 (includes EG:6822), GSTA1, CYP2C8, LC27A5, CYP3A7, ABCG5, ALDH8A1, APOC4 (includes EG:346), CYP3A4, ACSL1, ABCB11, FMO4, MAOA
Xenobiotic metabolism signaling	
Up	SULT1C2, PRKCD, GSTP1, MAPK13
Down	NR1I2, NR1I3, ALDH1L1, ABCB1, UGT2B15, MAP2K2, UGT2B7, PPARGC1A, GSTM1, PIK3C3, ALDH6A1, GSTM4, CES2 (includes EG:8824), MAP3K5, FMO3, PIK3C2G, SULT2A1 (includesEG:6822), CYP1A2, GSTA1, CYP2C8, CYP3A7, NQO2, ALDH8A1, CYP3A4, CES1 (includes EG:1066), FMO4, MAOA
Hepatic cholestasis	
Up	ADCY3, PRKCD
Down	CD14, ABCG5, NR1I2, CYP7A1, CYP7B, CYP8B1, ABCB1, ESR1, SLC10A1, ABCB11, ABCB4, HNF4A
Aryl hydrocarbon receptor signaling	
Up	GSTP1
Down	CDKN2A, NQO2, GSTM1, ALDH8A1, ALDH6A1, ALDH1L1, GSTM4, ESR1, CYP1A2, GSTA1, RARG
NRF2-mediated oxidative stress response	
Up	DNAJA4, PRKCD, GSTP1
Down	NQO2, GSTM1, AOX1, PIK3C3, GSTM4, MAP3K5, SOD1, PIK3C2G, MAP2K2, FKBP5, GSTA1
Complement system	
Up	
Down	C8A, C1R, MASP1, C6, C8B, MASP2
Coagulation system	
Up	
Down	SERPINC1, KLKB1, F9, KNG1 (includes EG:3827), F11
Acute-phase response signaling	
Up	MAPK13
Down	APCS, RBP5, C1R, MAP3K5, HRG, MAP2K2, KLKB1, SAA4
p53 signaling	
Up	THBS1
Down	CDKN2A, PIK3C3, SNAI2, GADD45A, PIK3C2G, GADD45B
LXR/RXR activation	
Up	HMGCR
Down	CD14, ABCG5, APOA5, CYP7A1, APOC4 (includes EG:346)

LXR/RXR, liver X receptor/retinoid X receptor; NRF2, NF-E2-related factor 2.
NOTE. The top 10 pathways were selected based on the significance for the enrichment of the genes with a particular canonical signaling pathway determined by the one-sided Fisher exact test ($P < .01$).

ELSEVIER

Journal of Hepatology 50 (2009) 100–110

Journal of Hepatology

www.elsevier.com/locate/jhep

Activation of lipogenic pathway correlates with cell proliferation and poor prognosis in hepatocellular carcinoma☆

Taro Yamashita[1], Masao Honda[1,2], Hajime Takatori[1], Ryuhei Nishino[1], Hiroshi Minato[3], Hiroyuki Takamura[4], Tetsuo Ohta[4], Shuichi Kaneko[1,*]

[1]*Department of Gastroenterology, Kanazawa University Graduate School of Medical Science, 13-1 Takara-Machi, Kanazawa 920-8641, Japan*
[2]*Department of Advanced Medical Technology, Kanazawa University School of Health Sciences, 13-1 Takara-Machi, Kanazawa 920-8641, Japan*
[3]*Pathology Section, Kanazawa University Hospital, 13-1 Takara-Machi, Kanazawa 920-8641, Japan*
[4]*Department of Gastroenterologic Surgery, Kanazawa University Graduate School of Medical Science, 13-1 Takara-Machi, Kanazawa 920-8641, Japan*

***Background/Aims*: Metabolic dysregulation is one of the risk factors for the development of hepatocellular carcinoma (HCC). We investigated the activated metabolic pathway in HCC to identify its role in HCC growth and mortality.**

***Methods*: Gene expression profiles of HCC tissues and non-cancerous liver tissues were obtained by serial analysis of gene expression. Pathway analysis was performed to characterize the metabolic pathway activated in HCC. Suppression of the activated pathway by RNA interference was used to evaluate its role in HCC *in vitro*. Relation of the pathway activation and prognosis was statistically examined.**

***Results*: A total of 289 transcripts were up- or down-regulated in HCC compared with non-cancerous liver ($P < 0.005$). Pathway analysis revealed that the lipogenic pathway regulated by sterol regulatory element binding factor 1 (*SREBF1*) was activated in HCC, which was validated by real-time RT-PCR. Suppression of *SREBF1* induced growth arrest and apoptosis whereas overexpression of *SREBF1* enhanced cell proliferation in human HCC cell lines. *SREBF1* protein expression was evaluated in 54 HCC samples by immunohistochemistry, and Kaplan–Meier survival analysis indicated that *SREBF1*-high HCC correlated with high mortality.**

***Conclusions*: The lipogenic pathway is activated in a subset of HCC and contributes to cell proliferation and prognosis.**

***Keywords*: Hepatocellular carcinoma; Serial analysis of gene expression; Lipogenesis; Gene expression profiling; Sterol regvulatory element binding factor 1**

Received 26 May 2008; received in revised form 1 July 2008; accepted 23 July 2008; available online 12 October 2008
Associate Editor: J.M. Llovet

☆ The authors who have taken part in the research of this paper declared that they do not have a relationship with the manufacturers of the materials involved either in the past or present and they did not receive funding from the manufacturers to carry out their research.

* Corresponding author. Tel.: +81 76 265 2231; fax: +81 76 234 4250.
E-mail address: skaneko@m-kanazawa.jp (S. Kaneko).

Abbreviations: HCC, hepatocellular carcinoma; *SREBF1*, sterol regulatory element binding factor 1; HBV, hepatitis B virus; HCV, hepatitis C virus; SAGE, serial analysis of gene expression; RT-PCR, reverse transcription-polymerase chain reaction; IHC, immunohistochemistry; FADS1, fatty acid desaturase 1; SCD, stearoyl CoA desaturase; FASN, fatty acid synthase; si-RNA, short interfering-RNA; CLD, chronic liver disease; PCNA, proliferating cell nuclear antigen; IGF, insulin-like growth factor.

1. Introduction

Hepatocellular carcinoma (HCC) is one of the most frequently occurring malignancies in the world [1]. The major risk factors associated with HCC include chronic infection with hepatitis B virus (HBV) and hepatitis C virus (HCV), alcohol abuse, and exposure to aflatoxin B1 [2]. HCC usually develops from liver cirrhosis, which involves continuous inflammation and hepatocyte regeneration, suggesting that reactive oxygen species and DNA damage are involved in the process of hepatocarcinogenesis [3].

The development of gene expression profiling technologies including DNA microarrays and serial analysis

0168-8278/$34.00
doi:10.1016/j.jhep.2008.07.036

of gene expression (SAGE) have enhanced our ability to identify inventory transcripts and global genetic alterations in HCC [4–10]. In general, these methods have demonstrated that transcripts associated with cell growth are up-regulated, whereas those related to inhibition of cell growth are down-regulated, in HCC [11]. It is difficult, however, to decipher molecular pathways activated during hepatocarcinogenesis.

Epidemiological studies suggest that metabolic dysregulation in the liver increases the risk of HCC development. For example, diabetes is associated with a 2-fold increase in the risk of HCC [12]. Obesity and hepatic steatosis also increase the risk of HCC [13–15]. Furthermore, recent studies indicate that HCV infection provokes hepatic steatosis, which may be a vulnerable factor for liver inflammation and HCC development [16,17]. Thus, dysregulation of a metabolic pathway may play a crucial role to promote HCC growth, but the molecular mechanism is still obscure. In this study, we have utilized SAGE [18,19], which enables us to monitor the differential expression of all genes, to determine the global changes in gene expression that occur during hepatocarcinogenesis.

2. Materials and methods

2.1. Tissue samples

All HCC tissues, adjacent non-cancerous liver tissues, and normal liver tissues were obtained from 69 patients who underwent hepatectomy from 1997 to 2005 in Kanazawa University Hospital. Normal liver tissue samples were obtained from patients undergoing surgical resection of the liver for treatment of metastatic colon cancer. HCC and surrounding non-cancerous liver samples were obtained from patients undergoing surgical resection of the liver for the treatment of HCC. The samples used for SAGE, real-time reverse-transcription (RT)-PCR analysis, and immunohistochemistry (IHC) are listed in Supplemental Table 1. All samples used for SAGE and real-time RT-PCR analysis were snap-frozen in liquid nitrogen. Four normal liver tissues and 20 HCCs and their corresponding non-cancerous liver tissues were used for real-time RT-PCR analysis; seven of these HCC samples, along with 47 additional HCC samples, were formalin-fixed paraffin-embedded and used for IHC. HCC and adjacent non-cancerous liver were histologically characterized as described [20].

All strategies used for gene expression analysis as well as tissue acquisition processes were approved by the Ethics Committee and the Institutional Review Board of Kanazawa University Hospital. All procedures and risks were explained verbally, and each patient provided written informed consent.

2.2. SAGE

Total RNA was purified from each homogenized tissue sample using a ToTally RNA extraction kit (Ambion, Inc., Austin, TX), and polyadenylated RNA was isolated using a MicroPoly (A) Pure kit (Ambion). A total of 2.5 μg mRNA per sample was analyzed by SAGE [18]. SAGE libraries were randomly sequenced at the Genomic Research Center (Shimadzu-Biotechnology, Kyoto, Japan), and the sequence files were analyzed with SAGE 2000 software. The size of each SAGE library was normalized to 300,000 transcripts per library, and the abundance of transcripts was compared by SAGE 2000 software. Monte Carlo simulation was used to select genes with significant differences in expression between two libraries without multiple hypothesis testing correction ($P < 0.005$) [21]. Each SAGE tag was annotated using a gene-mapping web site (http://www.ncbi.nlm.nih.gov/SAGE/index.cgi).

2.3. Analysis of signaling networks

Ingenuity Pathways Analysis software (Ingenuity® Systems, www.ingenuity.com) was used to investigate the molecular pathways activated in an HCC SAGE library compared with an adjacent non-cancerous liver SAGE library. All reliable transcripts statistically up-regulated in HCC were investigated and annotated with biological processes, protein-protein interactions, and gene regulatory networks, using a reference-based data file with statistical significance. All identified pathways were screened individually. MetaCore™ software (GeneGo Inc., St. Joseph, MI) was used to evaluate candidate transcription factors responsible for up-regulation of transcripts in HCC.

2.4. RT-PCR

A 1-μg aliquot of each total RNA was reverse-transcribed using SuperScript II reverse-transcriptase (Invitrogen, Carlsbad, CA). Real-time RT-PCR analysis was performed using ABI PRISM 7900 Sequence Detection System (Applied Biosystems, Foster City, CA). Using the standard curve method, quantitative **PCR** was performed in triplicate for each sample-primer set. Each sample was normalized relative to β-actin. The assay IDs used were Hs00231674_m1 for sterol regulatory element binding factor 1 (*SREBF1*); Hs00203685_m1 for fatty acid desaturase 1 (*FADS1*) ;Hs00748952_s1 for stearoyl CoA desaturase (*SCD*); Hs00188012_m1 for fatty acid synthase (*FASN*); and Hs99999_m1 for β-actin. *SREBF1a* and *SREBF1c* mRNA levels were assayed by semi-quantitative RT-PCR [22].

2.5. RNA Interference targeting SREBF1

Si-RNAs targeting *SREBF1* were constructed using a *Silencer*™ SiRNA Construction kit (Ambion) according to the manufacturer's protocol. We constructed two different si-RNAs, targeting different sites of *SREBF1* (*SREBF1*-1; CAGTGGCACTGACTCTTCC, *SREBF1*-2; TCTACGACCAGTGGGACTG). Control si-RNA duplexes targeting scramble sequences were also synthesized (Dharmacon Research, Inc., Lafayette, CO). Lipofectamine 2000™ reagent (Invitrogen) was used for transfection according to the manufacturer's instructions.

2.6. Cell proliferation assay

Cell proliferation assays were performed using a Cell Titer96 Aqueous kit (Promega, Madison, WI). Results are expressed as the mean optical density (OD) of each five-well set. All experiments were repeated at least twice.

2.7. Soft agar assay

To each well of a six-well plate, containing a base layer of 0.72% agar in growth medium, was added 1×10^4 cells, suspended in 2 ml of 0.36% agar with growth medium (DMEM supplemented with 10% FBS), and the plates were incubated at 37 °C in a 5% CO_2 incubator for 2 weeks. The numbers of colonies in each well were counted as previously described [23].

2.8. TUNEL assay

A DeadEnd™ Colorimetric TUNEL System (Promega) was used to measure nuclear DNA fragmentation as described previously [24].

2.9. Annexin V staining

To evaluate apoptotic cell death, Annexin V binding to cell membranes was evaluated using Annexin V-FITC antibodies and FACSCalibur flow cytometer (BD Biosciences, Franklin Lakes, NJ), as described by the manufacturer.

2.10. Focus assay

HuH7 cells and Hep3B cells were transiently transfected with pCMV7 or pCMV7-*SREBF1c* vectors (kindly provided by Dr. Hitoshi Shimano) using Lipofectamine 2000™ reagent (Invitrogen), as described by the manufacturer. A total of 2×10^3 cells were seeded on six-well plates 48 h after transfection, and cultured in usual media with 400 ng/ml of Geneticin for 9 days. The foci were fixed with ice-cold 100% methanol and stained with 0.5% crystal violet solution. All experiments were performed in triplicates.

2.11. Western blotting

Whole cell lysates were prepared using RIPA lysis buffer. Antibodies used were rabbit polyclonal antibodies to phospho-GSK-3β (ser9) (Cell Signaling Technology Inc., Danvers, MA), rabbit anti-sterol regulatory element binding protein-1 (encoded by *SREBF1*) polyclonal antibody H-160 (Santa Cruz Biotechnology, Inc., Santa Cruz, CA), and β-actin (Sigma–Aldrich Japan K.K., Tokyo, Japan). Immune complexes were visualized by enhanced chemiluminescence (Amersham Biosciences Corp., Piscataway, NJ) as described in the manufacturer's protocol.

2.12. Immunohistochemistry

Rabbit anti-*SREBF1* polyclonal antibody H-160 (Santa Cruz Biotechnology, Inc.) and mouse anti-proliferating cell nuclear antigen (PCNA) monoclonal antibody PC10 (Calbiochem, San Diego, CA) were used to evaluate the immunoreactivity of HCC samples, using a DAKO EnVision+™ Kit, as described by the manufacturer. The signal intensity of *SREBF1* was scored as negative, low, or high determined by the representative staining of the normal liver tissue and cirrhotic liver tissue (Supplemental Fig. 1). HCC was referred as *SREBF1*-high if *SREBF1* expression in the tumor was higher than that in the cirrhotic liver tissue. PCNA index was evaluated as previously described [25].

2.13. Statistical analysis

Kruskal–Wallis test was used to compare the differentially expressed genes, as shown by real-time PCR, among normal liver, CLD, and HCC tissues. Mann–Whitney U test was also used to evaluate the statistical significance of differences of gene expression between CLD and HCC tissues. Spearman's correlation coefficient was used to assess correlations between the expression levels of *SREBF1*, *FADS1*, *SCD*, and *FASN*. Univariate Cox proportional hazards regression analysis was used to evaluate the association of gene expression and clinicopathologic parameters with patient outcomes. All statistical analyses were performed using SPSS software (SPSS software package; SPSS Inc., Chicago, IL) and GraphPad Prism software (GraphPad Software Inc., La Jolla, CA).

3. Results

3.1. Gene expression profiling of HCC

We constructed two SAGE libraries from a HCC–HBV tissue and a corresponding non-cancerous tissue (chronic liver disease (CLD)–HBV). We also used two previously described SAGE libraries, from an HCC–HCV sample and a corresponding non-cancerous tissue sample (CLD–HCV) [4]. After excluding tags detected only once in each library, to avoid the contamination of tags derived from sequence errors, we selected 105,288 tags corresponding to the 9731 genes in all libraries. Using Monte Carlo simulation, we compared the differentially expressed transcripts in HCC and corresponding CLD libraries. Compared with their corresponding CLD libraries, there were statistically significant increases or decreases in 140 transcripts in the HCC–HBV library and in 197 transcripts in the HCC–HCV library ($P < 0.005$).

The HCC–HBV library contained one SAGE tag encoding the HBV–X region, which was increased more than 35-fold compared with its expression in the corresponding CLD–HBV library (Supplemental Table 2). We identified two additional SAGE tags, encoding unknown genes (GTTCTAAAGG, GCATTATGAT), which were expressed more than 10-fold in the HCC–HBV library than in the corresponding CLD–HBV library. The HCC–HBV library also contained tags associated with lipogenesis, at greater than 10-fold abundance, in the HCC–HBV library; these including tags for steroyl-CoA desaturase, fatty acid synthase, and fatty acid desaturase 1.

In contrast, SAGE tags associated with the immune response were up-regulated in the HCC–HCV library. These included tags for Th1-type chemokines, including chemokine ligand 10 (C–X–C motif), chemokine ligand 9 (C–X–C motif), and major histocompatibility complex classes IA and IB (Supplemental Table 3). In addition, tags associated with lipogenesis were increased in the HCC–HCV library, including tags for 3-hydroxy-3-methylglutaryl-coenzyme A synthase 1 and cytochrome P450, family 51, subfamily A, polypeptide 1. Taken together, the differential gene expression patterns may exist in HCC–HBV and HCC–HCV. HBV–X and lipogenesis-related genes are activated in HCC–HBV, whereas genes associated with inflammation as well as lipogenesis are activated in HCC–HCV.

3.2. Analysis of molecular pathways activated in HCC

To further characterize the gene expression patterns of HCC–HBV and HCC–HCV, we performed pathway analysis on SAGE data. Using MetaCore™ software, we found that the candidate transcription factors activated were distinct in each HCC library (Table 1). Several of these transcription factors, including NF-κB, c-Myc, c-Jun, and HNF4-α, have been reported to be activated in HCC [26–29]. In addition, our findings indicated that the transcription factor *SREBF1* may be activated in both HCC–HBV and HCC–HCV (to avoid a confusion, we use HUGO symbol *SREBF1* to indicate both gene/protein name).

Table 1
Candidate transcription factors that regulate molecular pathways activated in HCC.

SAGE library	Transcription factor	Molecular processes	*P*-value
HCC–HCV	NF-κB	Antigen presentation Antigen processing Defense response Immune response	0.004
	SREBF1	Cholesterol biosynthesis Lipid biosynthesis β-Glucoside transport Negative regulation of lipoprotein metabolism	0.05
	SP1	Electron transport; drug metabolism Oxygen and reactive oxygen species metabolism Cell-substrate junction assembly; wound healing	0.05
	IRF1	Immune response Antigen presentation; antigen processing Defense response; positive regulation of cell	0.05
HCC–HBV	HNF4-α	Lipid transport Fatty acid metabolism Smooth muscle cell proliferation	0.002
	HNF1	Acute-phase response; lipid transport Negative regulation of lipid catabolism β-Glucoside transport Negative regulation of lipoprotein metabolism	0.01
	SP1	Zinc ion homeostasis; response to biotic stimulus Nitric oxide mediated signal transduction Copper ion homeostasis; fatty acid biosynthesis	0.01
	c-Jun	Progesterone catabolism; progesterone metabolism Regulation of lipid metabolism; Prostaglandin metabolism	0.03
	C/EBP-α	Lipid transport; negative regulation of lipid catabolism Negative regulation of lipoprotein metabolism β-Glucoside transport Positive regulation of interleukin-8 biosynthesis	0.03
	SREBF1	Lipid biosynthesis; fatty acid biosynthesis Fatty acid metabolism Negative regulation of lipid catabolism Negative regulation of lipoprotein metabolism	0.03
	c-Myc	Fatty acid biosynthesis; fatty acid metabolism Fatty acid desaturation; Activation of pro-apoptotic gene products Release of cytochrome c from mitochondria	0.03
	USF1	Fatty acid metabolism Smooth muscle cell proliferation	0.03
	PPAR-α	Fatty acid metabolism Smooth muscle cell proliferation	0.03
	COUP-TFI	Lipid transport Smooth muscle cell proliferation	0.03
	C/EBP-β	Acute-phase response Regulation of interleukin-6 biosynthesis Fat cell differentiation Inflammatory response	0.03

These findings were evaluated by other pathway analysis software, Ingenuity Pathways Analysis (IPA). We applied the signaling network analysis to the transcripts up-regulated in the HCC libraries ($P < 0.005$). We found that the top signaling network activated in HCC–HBV contained several pathways involved in ERK/MAPK signaling, PPAR signaling, linoleic acid metabolism, and fatty acid metabolism (Supplemental Fig. 2A). Similarly, pathways involved in interferon signaling, NF-κB signaling, antigen presentation, PPAR signaling, linoleic acid metabolism, and fatty acid metabolism were included in the top signaling network activated in HCC–HCV (Supplemental Fig. 2B). Consistent with the results of transcription factor analysis by MetaCore™, pathway analysis indicated that *SREBF1* participates in the lipogenesis pathway in both HCC–HBV and HCC–HCV (blue nodes in Supplemental Fig. 2A and B). *SREBF1*, a major regulator of the lipogenesis pathway, binds to sterol regulatory elements on the genome [30], but less is known about its role in

HCC [31]. We therefore focused on the role of *SREBF1* signaling in HCC.

3.3. Validation of SAGE and signaling network analysis

We performed real-time RT-PCR analysis of *SREBF1* and three representative target genes (*SCD*, *FADS1*, and *FASN*) [20] on 44 samples not used for SAGE. We found that the levels of *SREBF1*, *SCD*, and *FASN* mRNAs were higher in HCC tissues and CLD tissues compared with normal liver, and that these differences were statistically significant (Fig. 1A). We further compared the expression of *SREBF1*, *FADS1*, and *FASN* between HCC and non-cancerous liver tissues, and identified the overexpression of *SREBF1* in HCC with statistical significance (Supplemental Fig. 3). Scatter plot analysis showed that the expression levels of *SREBF1* were correlated with those of *FADS1* ($R = 0.57$, $P < 0.0001$), *SCD* ($R = 0.82$, $P < 0.0001$), and *FASN* ($R = 0.74$, $P < 0.0001$) (Fig. 1B).

Since the mammalian genome encodes two *SREBF1* isoforms, *SREBF1a* and *SREBF1c* [22], we performed semi-quantitative RT-PCR with isoform specific primers to determine which of these isoforms was up-regulated in HCC. We found that *SREBF1c* mRNA, but not *SREBF1a* mRNA, was up-regulated in HCC compared with adjacent non-cancerous liver and normal liver tissues (Supplemental Fig. 4A).

3.4. Functional assay of the lipogenesis pathway in cell lines

Although genome-wide expression profiling showed that the lipogenesis pathway was activated in HCC possibly through up-regulation of *SREBF1*, it was not clear that this pathway played a role in HCC growth. To investigate the role of lipogenesis in HCC cell proliferation, we transfected two short interfering (si)-RNAs (*SREBF1*-1 and *SREBF1*-2) targeting *SREBF1* into the HuH7 and Hep3B cells. These cell lines have no chromosome amplification or deletion on 17p11, on which *SREBF1* is located [32]. Transfection of the si-RNA constructs for *SREBF1*-1 or *SREBF1*-2 decreased expression of *SREBF1* 90% and 70%, respectively, and the expression of both *SCD* and *FADS1* 70% and 60%, respectively (Fig. 2A). Because differences in *SREBF1c* and *SREBF1a* *sequence alignments* are very small, we could not design si-RNAs specifically targeting *SREBF1c*. We therefore checked the effect of si-RNAs on the expression of the *SREBF1* isoforms. We found that the expression of *SREBF1c* was relatively more suppressed than that of *SREBF1a* (Supplemental Fig. 4B), which may have been associated with the higher expression of *SREBF1a* than *SREBF1c* in cultured cell lines [25].

We found that the growth of these transfected cells was significantly inhibited at 72 h compared with mock transfected cells (Fig. 2B and Supplemental Fig.5A). Examination of anchorage independent cell growth showed strong suppression by deactivation of the lipogenesis pathway (Fig. 2C). Because insulin-like growth factor (IGF) is known to induce cancer cell proliferation through activation of PI3-kinase signaling followed by *SREBF1* induction, we investigated the effect of *SREBF1* knockdown on IGF2 mediated cell proliferation. Interestingly, *SREBF1* knockdown abrogated the IGF2 dependent cell proliferation (Supplemental Fig. 5B). Moreover, both the TUNEL assay and annexin V staining showed that transfection of *SREBF1* si-RNAs increased apoptosis compared with mock transfected cells (Fig. 2D and E).

We further investigated the role of *SREBF1* overexpression on cell growth *in vitro*. We transiently transfected control pCMV7 plasmids or pCMV7-*SREBF1c* plasmids (Fig. 3A), and cell proliferation was enhanced in *SREBF1* overexpressing cells compared with the control in both HuH7 and Hep3B cells evaluated by focus assay (Fig. 3B and supplemental Fig. 6). Furthermore, overexpression of *SREBF1* intensified the phosphorylation of GSK-3β, one of the major kinase phosphorylated by the activation of IGF signaling, in a dose-dependent manner (Fig. 3C).

3.5. SREBF1 Expression and prognosis

Since the above results indicated that *SREBF1* signaling may play an important role on tumor cell growth, we investigated the relationship between *SREBF1* expression and mortality in 54 HCC patients by IHC. When we examined the expression of *SREBF1* in HCC tissues and adjacent non-cancerous liver tissues, we identified the increase of the cytoplasmic *SREBF1* staining in a subset of HCC (Fig. 4A). We evaluated the expression of *SREBF1* in HCC and classified 4, 30, and 20 HCCs as *SREBF1*-negative, *SREBF1*-low, and *SREBF1*-high HCC, respectively (Fig. 4B and Supplemental Fig. 1). We could not detect any differences of clinico-pathological characteristics between *SREBF1*-high HCC and *SREBF1*-low/-negative HCC including histological steatosis (Supplemental Table4). Since the seven of these HCC samples were also used for real-time RT-PCR analysis, we investigated the relation of *SREBF1* RNA and protein expression (Fig. 4C). *SREBF1*RNA expression was significantly higher in *SREBF1*-high HCC than in *SREBF1*-low/-negative HCC with statistical significance ($P = 0.03$). Then we examined the cell proliferation of these HCC samples by PCNA staining. Notably, PCNA indexes were significantly higher in *SREBF1*-high HCC than *SREBF1*-low/-negative HCC with statistical significance ($P < 0.001$) (Fig. 4D). We further investigated the relationship between *SREBF1*

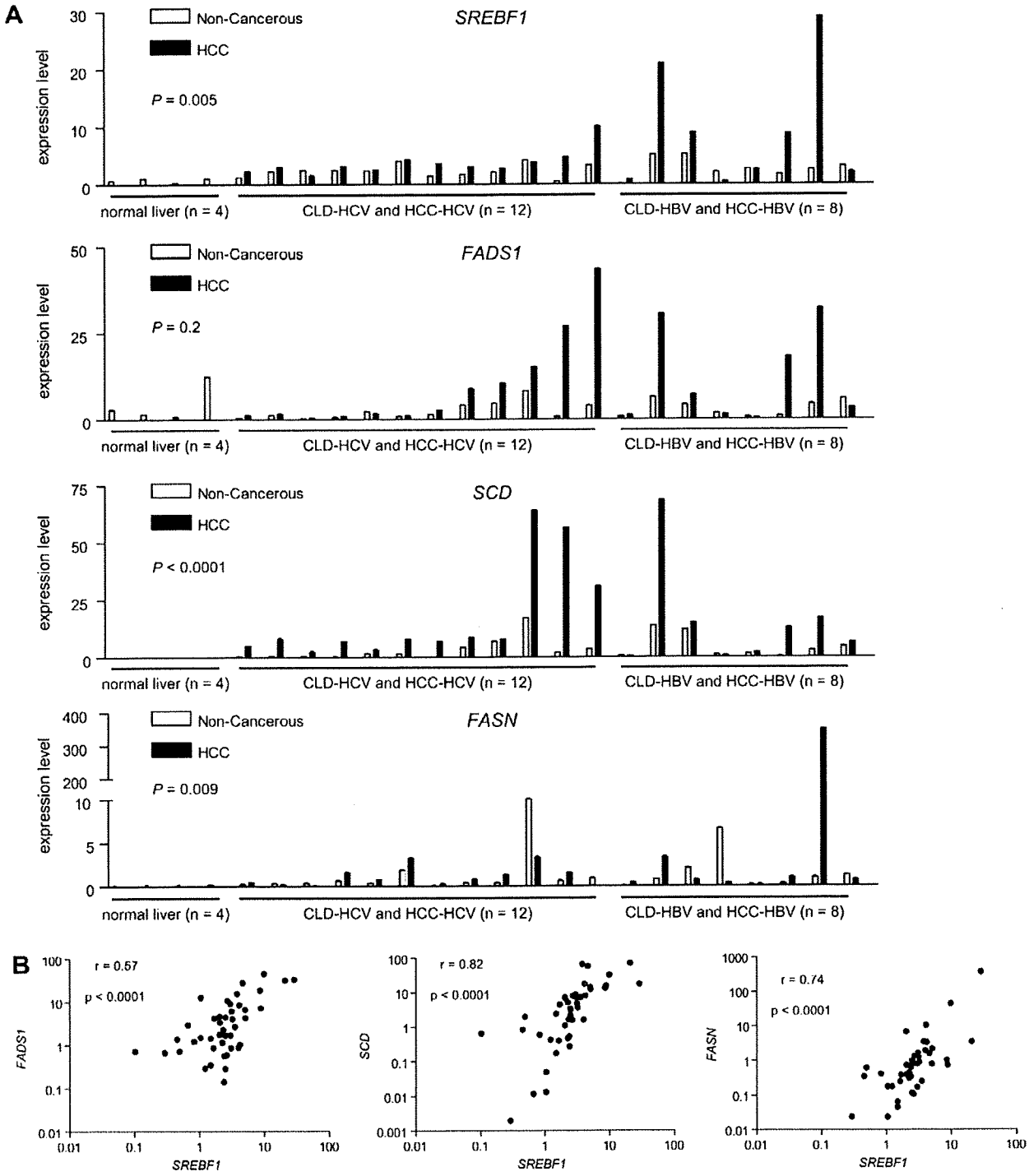

Fig. 1. (A) Real-time quantitative RT-PCR analysis. RNA was isolated from 44 tissue samples: 20 HCC, 20 corresponding CLD, and four normal liver samples. Differential expression of each gene among normal liver tissues, CLD tissues, and HCC tissues was examined by Kruskal–Wallis tests. (B) Scatter plot analysis. Gene expression levels of *FADS1*, *SCD* and *FASN* were well-correlated with those of *SREBF1*, as shown by Spearman's correlation coefficients.

protein expression and prognosis. Kaplan–Meier survival analysis showed a significant relationship between poor survival and high *SREBF1* protein expression ($P = 0.04$; Fig. 4E). Univariate Cox regression analysis showed a correlation between high *SREBF1* protein expression and high risk of mortality with statistical

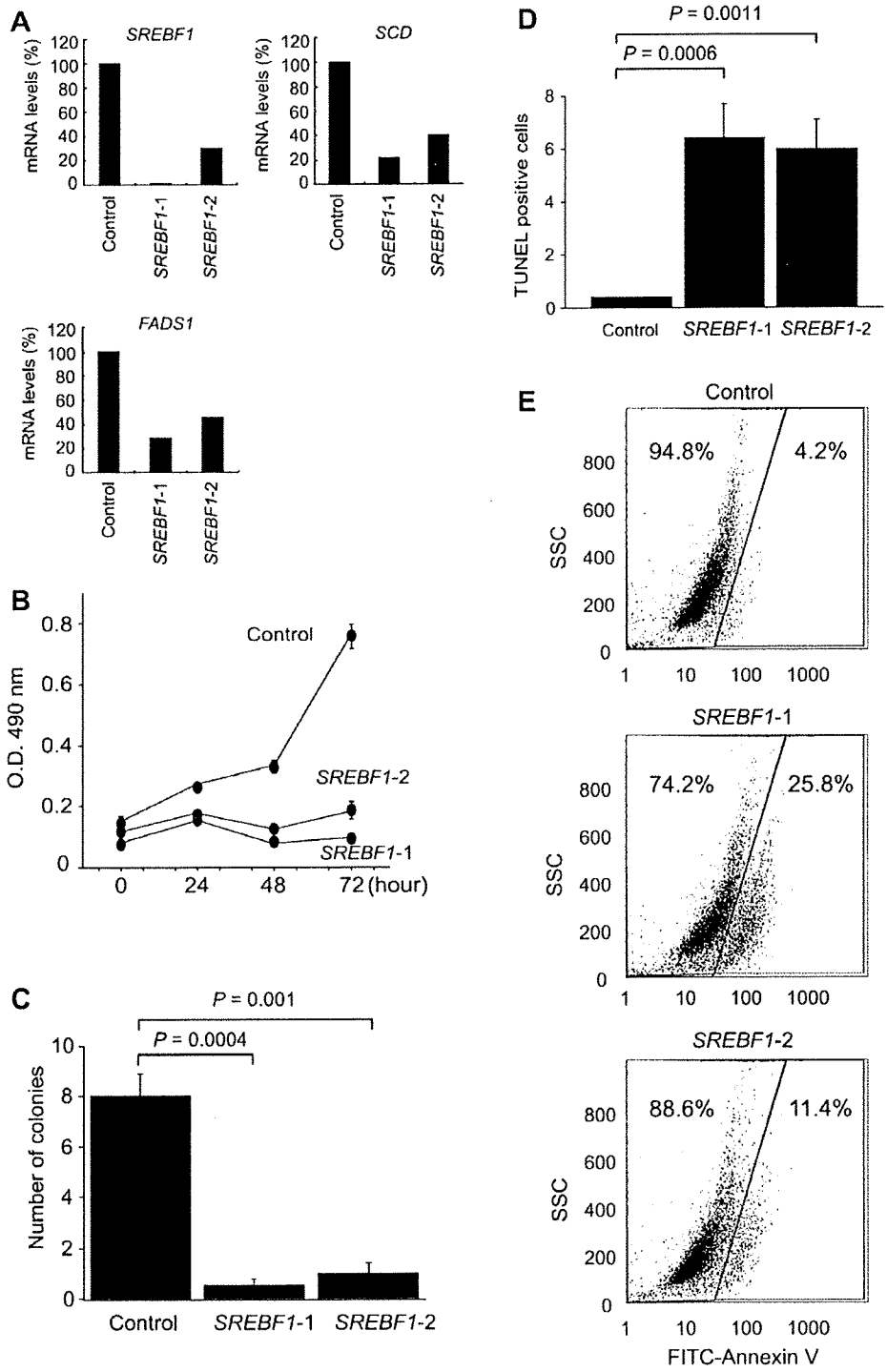

Fig. 2. (A) Effect of RNA interference targeting *SREBF1* in HuH7 cells. Expression levels of *SREBF1* mRNA were reduced by si-RNAs targeting different exons in *SREBF1*. Transcripts of *FADS1* and *SCD* were also down-regulated, showing transcriptional deactivation of the lipogenesis pathway. (B) Cell proliferation assay. Deactivation of the lipogenesis pathway severely reduced cell growth in HuH7 cells. (C) Soft agar assay. Deactivation of the lipogenesis pathway inhibited anchorage independent cell growth in HuH7 cells. (D) TUNEL assay. Deactivation of the lipogenesis pathway significantly increased the number of TUNEL-positive cells in HuH7 cells. (E) Annexin V staining evaluated by flow cytometer. Deactivation of the lipogenesis pathway significantly increased the number of annexin V positive cells in HuH7 cells.

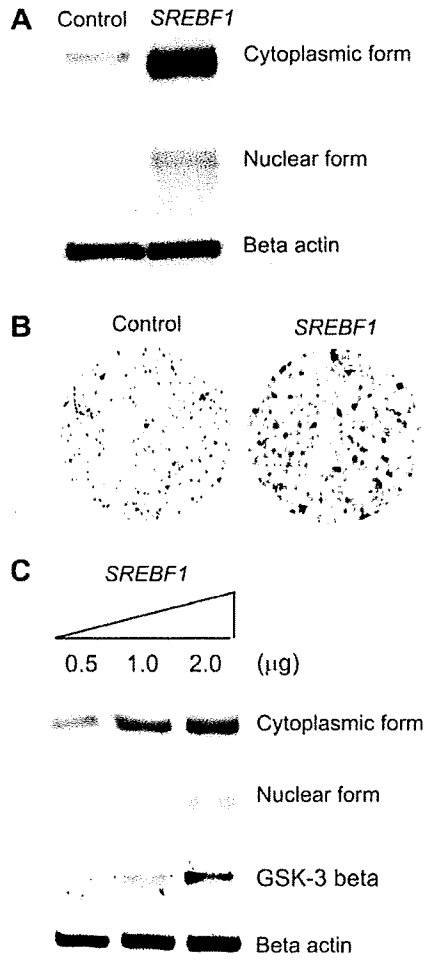

Fig. 3. (A) Western blot analysis of *SREBF1* protein expression in HuH7 cells transfected with control pCMV7 plasmids or pCMV7-*SREBF1c* plasmids. Both cytoplasmic and nuclear forms of *SREBF1* protein expression were increased by pCMV7-*SREBF1c* overexpression. (B) Focus assay of HuH7 cells transfected with control pCMV7 plasmids or pCMV7-*SREBF1c* plasmids. (C) Western blot analysis of *SREBF1* and phospho-GSK-3β protein expression in HuH7 cells transfected with indicated amounts of pCMV7-*SREBF1c* plasmids.

significance (HR, 3.7; 95% CI, 1.0–13.7; $P = 0.05$; Table 2).

4. Discussion

Using large-scale gene expression profiling, we have shown that the lipogenesis pathway is transcriptionally activated in HCC. Our SAGE profiles will be available on our homepage (http://www.intmedkanazawa.jp/) and will be submitted to the Gene Expression Omnibus (http://www.ncbi.nlm.nih.gov/geo/).

We found that the levels of expression of *FADS1*, *SCD*, and *FASN* were each correlated with those of *SREBF1*, suggesting that *SREBF1* is one of the main factors involved in the activation of lipogenesis in HCC. Activation of growth signaling pathways, such as the PI 3-kinase and mitogen-activated protein kinase pathways, has been shown to induce up-regulation of *SREBF1* in prostate and breast cancer cells [33,34]. We have observed induction of *SREBF1* protein expression by IGF2 in HuH7 cells (data not shown). Furthermore, we have identified that *SREBF1* overexpression results in the activation of cell proliferation and PI 3-kinase signaling, whereas expression inhibition of *SREBF1* abrogated the IGF2 induced cell proliferation. Although detailed mechanisms should be clarified in future, our results suggest that *SREBF1* is a key component of PI 3-kinase signaling in HCC.

SREBF1 is induced by alcohol [35], insulin, and fat [30,36], and plays a central role in the mechanism of hepatic steatosis [37]. Interestingly, these *SREBF1* inducers are risk factors for HCC [12,13,38,14]. Strikingly, two recent studies have shown that HBV and HCV infection may also induce hepatic steatosis through activation of *SREBF1* [39,40]. Furthermore, a recent report revealed the activation of *SREBF1* signaling in cancer by hypoxia [41]. Thus, these pathologic conditions such as chronic viral hepatitis, alcohol abuse, obesity, diabetes, and local hypoxia may up-regulate the expression of *SREBF1*, which, in turn, may contribute to an increased risk of hepatocarcinogenesis. Transgenic mice overexpressing *SREBF1* in the liver exhibited hepatic steatosis and hepatomegaly, suggesting the role of *SREBF1* on lipid metabolism and cell proliferation. However, it should be noted that no transgenic mice overexpressing *SREBF1* have been reported to have the risk of HCC development thus far. Interestingly, a recent report indicated that HCV core transgenic mice known to develop HCC showed coordinated activation of lipogenic pathway genes and *SREBF1* [42]. Although further studies are clearly required, we speculate that the activation of *SREBF1* may contribute to promote the development of HCC in already-initiated hepatocytes but not in normal hepatocytes.

Recently, Yahagi et al. reported the activation of lipogenic enzyme related genes in HCC [31]. In that paper, the authors suggested that *SREBF1* expression was not correlated with the expression of other lipogenic genes by Northern blotting, inconsistent with our current data. One possible explanation of these discrepancies might be the different methods for quantitation of mRNA, and we believe that real-time RT-PCR method used in our study would be more accurate. In addition, we evaluated the expression of *SREBF1* and lipogenic genes using more samples (a total of 44 liver and HCC tissues) than Yahagi et al did (10 HCC tissues). Furthermore, a recent paper indicated the coordinated activation of *SREBF1* and lipogenic genes in HCC

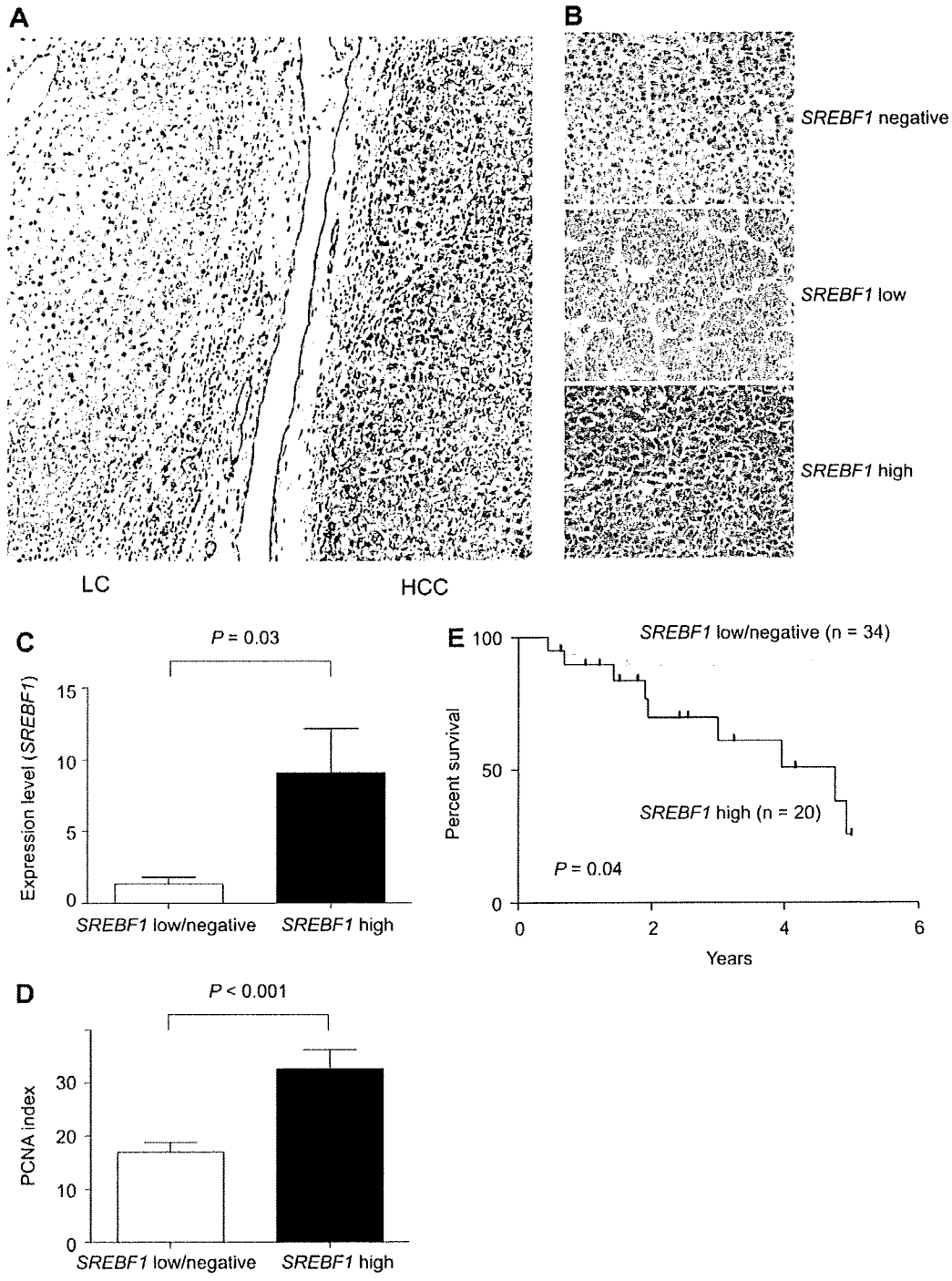

Fig. 4. (A) A photomicrograph of an HCC with adjacent non-cancerous cirrhotic liver stained with anti-*SREBF1* antibodies. (B) Representative photomicrographs of *SREBF1*-negative-, *SREBF1*-low-, and *SREBF1*-high-HCC tissues stained with anti- *SREBF1* antibodies. (C) *SREBF1* gene expression by real-time RT-PCR according to protein expression status assessed by IHC. *SREBF1* was highly expressed in *SREBF1*-high HCC ($P = 0.03$). (D) SREBF1 expression and cell proliferation in HCC. PCNA indexes in *SREBF1*-high HCC were higher than those in *SREBF1*-low/-negative HCC with statistical significance ($P < 0.001$). (E) Kaplan–Meier plots of 54 HCC patients analyzed by immunohistochemistry. The differences between *SREBF1*-high and -low/-negative HCC were analyzed by log-rank test.

developed in the liver of HCV core transgenic mice [42], strongly support our data. Although further studies using large numbers of HCC tissues may be required, these data suggest that the lipogenic gene activation seems to be mediated, at least in part, by *SREBF1* expression in HCC.